Published in final edited form as:
Mol Microbiol. 2008 October ; 70(2): 352–368. doi:10.1111/j.1365-2958.2008.06410.x.

Histoplasma capsulatum secreted γ-glutamyltransferase reduces iron by generating an efficient ferric reductant

Robert Zarnowski[1,*], **Kendal G. Cooper**[1], **Laura Schmitt Brunold**[1], **Jimmy Calaycay**[2], and **Jon P. Woods**[1,*]

1*Department of Medical Microbiology and Immunology, University of Wisconsin, Madison, WI*

2*Protein Structure Laboratory, Department of Biochemistry, SUNY Downstate Medical Center, Brooklyn, NY*

Summary

The intracellular fungal pathogen *Histoplasma capsulatum* (Hc) resides in mammalian macrophages and causes respiratory and systemic disease. Iron limitation is an important host antimicrobial defense, and iron acquisition is critical for microbial pathogenesis. Hc displays several iron acquisition mechanisms, including secreted glutathione-dependent ferric reductase activity (GSH-FeR). We purified this enzyme from culture supernatant and identified a novel extracellular iron reduction strategy involving γ-glutamyltransferase (Ggt1) activity. The 320-kDa complex was composed of glycosylated protein subunits of about 50 and 37 kDa. The purified enzyme exhibited γ-glutamyl transfer activity as well as iron reduction activity in the presence of glutathione. We cloned and manipulated expression of the encoding gene. Overexpression or RNAi silencing affected both GGT and GSH-FeR activities concurrently. Enzyme inhibition experiments showed the activity is complex and involves two reactions. First, Ggt1 initiates enzymatic breakdown of GSH by cleavage of the γ-glutamyl bond and release of cysteinylglycine. Second, the thiol group of the released dipeptide reduces ferric to ferrous iron. A combination of kinetic properties of both reactions resulted in efficient iron reduction over a broad pH range. Our findings provide novel insight into Hc iron acquisition strategies and reveal a unique aspect of Ggt1 function in this dimorphic mycopathogen.

Keywords

Iron acquisition; pathogenesis; fungus; dimorphism; GGT

Introduction

Iron is an indispensable micronutrient for nearly all living organisms, where it acts as a cofactor of many enzymes involved in manifold vital cellular and physiological functions. In a mammalian host, iron is mainly maintained bound to highly specialized iron transport and iron storage proteins such as transferrin, lactoferrin and ferritin, and is sequestered in response to microbial infections. This essentially allows eliminating labile iron from plasma and extracellular tissues of the host, whereas the remaining pool of the metal can be ultimately bound to negatively charged molecules such as albumin. This system permits the mammalian host to maintain access to the metal in a soluble but non-reactive state while preventing the invading bacterial and fungal pathogens from acquiring iron and, consequently, from successful parasitism. Thus, iron has been implicated to have a critical role in infectious

*Correspondence: Dr Jon P. Woods. Tel: +1 608 265-6292. Fax: +1 608 265-6717. E-mail: jpwoods@wisc.edu. Dr Robert Zarnowski. Tel. (+1) 608 265-6228. Fax. (+1) 608 265-6717. E-mail: rzarnowski@wisc.edu.

diseases (Weinberg, 1999; Jung and Kronstad, 2007). On the other hand, excessive amounts of liberated iron may have certain hazardous implications. Iron overload severely compromises the iron withholding-based host defense strategy and likely contributes to the increase in susceptibility to some fungal and bacterial infections (Bullen *et al.*, 2006). There is also evidence that excessive amounts of this element impair the ability of phagocytes to kill invading pathogenic microorganisms (Appelberg, 2006). In addition, iron has the ability to initiate and catalyze the Fenton chemistry reactions, which lead to the formation of free oxygen radicals (Valko *et al.*, 2005). These unstable molecules are highly reactive and can initiate cascades of lethal reactions in both the host and the infectious microorganism. As a consequence of all these properties, microbial pathogens have to compete for iron in the host so that they can multiply and establish a successful infection, but they also have to control and regulate iron acquisition tightly to prevent accumulation of excessive amounts of this metal (Kosman, 2003).

Histoplasma capsulatum has solved the problem of iron solubilization and acquisition aptly by expressing a plethora of strategies to obtain iron. *H. capsulatum* is a human mycopathogen causing a deep systemic mycosis called histoplasmosis. This common systemic human mycosis is endemic in certain areas of North and Latin America, but cases have been diagnosed worldwide. In the United States, most cases have been reported within the Ohio and Mississippi River valleys (Wheat, 2003). Progressive disseminated histoplasmosis is a severe respiratory and systemic disease, mostly of the reticuloendothelial system, manifesting itself in the lungs, bone marrow, liver, and the spleen. The fungus enters and multiplies within human pulmonary macrophages in a unique phagosomal or phagolysosomal compartment, where it modulates, but does not completely reverse or block compartment acidification and maintains a pH of approximately 6.5 (Newman *et al.*, 2006). Iron is definitely needed for both intracellular (Lane *et al.*, 1991, Newman *et al.*, 1994, 1995) and *in vitro* growth of *H. capsulatum* (Timmerman and Woods, 1999, 2001).

There are two general types of iron acquisition mechanisms utilized by *H. capsulatum*. The first strategy relies on iron uptake before reduction and requires the presence of low molecular weight iron chelators called siderophores (Howard, 1999; Hwang *et al.*, 2008). *H. capsulatum* has been reported to produce hydroxamate siderophores during mycelial and yeast phase growth in iron-deplete media (Holzberg and Artis, 1983; Howard *et al.*, 2000). The fungus can also utilize xenosiderophores produced by other microbes (Timmerman and Woods, 2001). An alternative non-reductive route to acquire iron involves its gradual release from transferrin at acidic pH (Newman *et al.*, 2006) as well as cell wall-associated hemin binding (Foster, 2002).

The other strategy for iron uptake starts with extracellular iron reduction that can be catalyzed in the presence of specific iron reductases or secreted external low weight molecular reductants (de Luca and Wood, 2000). Reduction of ferric to ferrous iron followed by the transport of the latter form into the fungal cell may provide an effective way to acquire iron from both inorganic and organic ferric salts, from Fe^{3+}-loaded siderophores, or from host Fe^{3+}-binding proteins. In *H. capsulatum*, three iron-reducing activities are expressed: glutathione-dependent ferric reductase (GSH-FeR), low-molecular-weight non-enzymatic reductants, and cell surface reducing activity (Timmerman and Woods, 1999). GSH-FeR was characterized as a proteinase K-susceptible, heat-labile secreted protein present in high molecular fraction of supernatant (Timmerman and Woods, 1999). This enzyme could reduce iron bound to siderophores and to iron binding proteins such as transferrin or hemin (Timmerman and Woods, 2001). GSH-FeR required GSH for its activity (Timmerman and Woods, 1999) and could be reversibly inhibited by trivalent non-reducible iron analogues aluminum and gallium (Zarnowski and Woods, 2005). The present study was undertaken to identify GSH-FeR and to determine a mechanism of extracellular iron reduction in *H. capsulatum*. We present evidence that *H. capsulatum*

secreted γ-glutamyltransferase (Ggt1) plays a key role in the process of extracellular enzymatic iron reduction. Finally, we demonstrate that extracellular iron reduction is a complex process, which might function efficiently within the intracellular macrophage milieu infected with *H. capsulatum*.

Results

Initial purification and identification of GSH-FeR

GSH-FeR was partly purified from concentrated culture supernatants by a combination of chromatography techniques including ion exchange chromatography, size exclusion chromatography, and chromatofocusing. Iron reductase-positive fractions were pooled, concentrated and directly subjected to trypsin digestion followed by mass spectrometry-assisted internal amino acid sequencing. The initial purification strategy used yielded a sample containing 1.2 μg protein and was a mixture of three proteins, one of which was subsequently identified as GSH-FeR. The analysis of the trypsin-generated peptide masses by tandem mass spectrometry followed by database searches revealed two major peptides detected, LGLGDTITR and IITGTVQSVINLLDR, matching the protein sequence of γ-glutamyltransferase (*GGT1*; E.C. 2.3.2.2). A nucleotide sequence of a putative *GGT1* gene was found in the HISTO_ZY.Contig004 in the genome of *H. capsulatum* G217B strain (Washington University; http://www.genome.wustl.edu/tools/blast/). In addition, genomic *GGT1* sequences were identified in the contig5.9 in the genome of *H. capsulatum* G186AR strain (Washington University) as well as in the locus HCAG_03238.1 of the supercontig 3 in the genome of *H. capsulatum* WU24 strain (Broad Institute, MIT; http://www.broad.mit.edu/annotation/genome/histoplasma_capsulatum/Blast.html). In order to define a start codon of the *H. capsulatum GGT1*, these putative genomic sequences were used to search on-line available nucleotide and protein databases of other fungal species. BLAST searches showed 61 % identity and 76 % similarity to *Coccidioides immitis GGT* as well as to genes located in genomes of various aspergilli. Intriguingly, *GGT* found in the genome of *Aspergillus terreus* was considerably longer and its putative start codon was located much further upstream in comparison to other *GGT* genes. Since homologies to *Coccidioides* and *Aspergillus* GGTs were based only on gene predictions and GGT homologous proteins have not been functionally confirmed or characterized in these fungi, we used them to provide frameworks for delineating the *H. capsulatum* sequence. We identified two putative *GGT1* ORF sequences, (ORF1 and ORF2 shown in Fig. 1A) for use in expression cloning. Both ORF sequences contained putative translation start codons ATG. One potential *GGT1* ORF, corresponding to the *Coccidioides* homolog, consisted of 1518 nucleotides, whereas the second sequence was an upstream-extended variant harboring an extra 240 nucleotides (1758 bp after an intron splicing event of the 2421-bp genomic DNA fragment), corresponding to the *A. terreus* homolog. Using these two sequences, two pairs of oligonucleotides were designed (*GGT1*.AscI.ORF1.F and *GGT1*.SbfI.ORF1.R for ORF1, and *GGT1*.AscI.ORF2.F and *GGT1*.SbfI.ORF1.R for ORF2, respectively) (Table 1) and were used for PCR amplification and subsequent cloning into the pLBZ1 plasmid as described below. Both PCR-amplified putative *GGT1* ORFs were cloned into respective overexpression vectors, which subsequently were electroporated into a uracil-auxotrophic *H. capsulatum* G217B*ura5-23* strain (Woods *et al.*, 1998). The following screening of recovered transformants revealed a significant increase in Ggt1 activity, but only in the fungi episomally expressing the extended 1758-bp cDNA fragment (ORF2), indicating, thereby, we had properly identified the *H. capsulatum GGT1* gene. Subsequent DNA sequencing and bioinformatics-based gene structure prediction analyses showed that the *GGT1* gene of *H. capsulatum* G217B is organized into 6 exons of diverse length (Fig. 1A). This sequence generates the predicted 1758-bp transcript and exactly the same size could be observed after *GGT1* amplification from cDNA (Fig. 1B). In turn, this transcript encodes a predicted 586-aa preproprotein of 63.1 kDa,

which contains a predicted 28-amino acid secretion signal sequence and 12 putative N-glycosylation sites in its structure.

Purification and biochemical characterization of Ggt1

To purify and assess biochemical properties of Ggt1, the enzyme was overexpressed under the control of a constitutive *H. capsulatum*-native promoter. Purification of heterologously expressed Ggt1 was done using the same purification strategy as described above, which yielded considerably more of the pure protein (Fig. 2A). The recovery corresponded to 5.3 % of the initial enzymatic activity and its specific activity increased 1304-fold (Table 2). On a native PAGE gel, the purified Ggt1 occurred as a very large glycoprotein complex (Fig. 2B); however subsequent high-performance chromatographic separation on a set of two Superdex 200 columns allowed a precise size of Ggt1 to be determined at 320 ± 10 % kDa. On a SDS-PAGE gel after gel filtration, the Ggt1 preparation appeared pure with two apparent equally glycosylated bands at about 50 and 37 kDa, which is a common feature of all known GGT-type enzymes (Fig. 2C). Chromatofocusing of the purified enzyme determined its isoelectrofocusing point (pI) at 4.8 (Fig. 2D).

GGTs constitute a fairly large and ubiquitous group of enzymes involved in transpeptidation reactions, in which a γ-glutamyl residue is transferred from γ-glutamyl compounds to various acceptor molecules, such as amino acids, peptides or water (Kinlough *et al.*, 2005). In the latter case, this reaction is classified as hydrolysis. The existence of considerable discrepancies in catalytic properties between GGTs of different origins has been well documented showing certain preferences towards transpeptidation, hydrolysis or both reaction types (Ikeda *et al.*, 1995; Hiratake, 2005; Boanca *et al.*, 2006). To evaluate enzymatic properties of Ggt1 isolated from *H.capsulatum* cultures, we used a non-physiological substrate analogue γ-glutamyl-*p*-nitroanilide (GpNA) as an artificial donor of glutamyl residues. GpNA is the substrate employed in most GGT studies and its decomposition in the presence of Ggt1 can be monitored spectrophotometrically at 412 nm. We also applied 20 mM glycylglycine, which acted as an acceptor of glutamyl groups in the reaction of transpeptidation. Measurements to determine kinetic constants, K_m and V_{max}, were carried out using purified Ggt1 incubated with increasing concentrations of GpNA and, in the case of glutamyl transfer reaction, with glycylglycine added.

Saturation kinetics were observed and the data were then processed using non-linear regression analysis. There was significant pH dependence for kinetics constants, V_{max} and K_m, but differences in hydrolysis and transpeptidation activities of Ggt1 were rather marginal (Fig. 3). The highest Ggt1 activity in the GpNA hydrolysis was observed at neutral and slightly alkaline pH and the apparent average V_{max} was 66.34 ± 0.77 μmol min^{-1} (mg GGT)$^{-1}$, whereas the apparent optimal K_m for GpNA was about 0.75 ± 0.02 mM. Glutamyl transfer reaction in the presence of 20 mM glycylglycine was slightly slower with the calculated apparent V_{max} of 64.83 ± 0.77 μmol min^{-1} (mg Ggt1)$^{-1}$ and the apparent optimal K_m for GpNA of about 0.84 ± 0.02 mM. Mass spectrometric analysis confirmed that the reaction of transpeptidation occurred, as a molecular peak corresponding to the molecular mass of glutamylglycylglycine was detected.

Ggt1 is involved in extracellular iron reduction in H. capsulatum

To assess the role of Ggt1 in extracellular iron reduction, a panel of *H. capsulatum* G217B mutants with altered *GGT1* expression/activity levels was created. A strain bearing an empty pLBZ1 vector was used as a control. There was no difference in Ggt1 activity observed between the wild type G217B strain and the empty vector control transformant. Upregulation of the Ggt1 activity was achieved by expressing the *GGT1* gene under the constitutive *H. capsulatum*-native *H2B* promoter (Bohse and Woods, 2007), which provided a considerable,

about six-fold increase in the enzyme activity when measured in high-molecular weight supernatant fraction (Fig. 4A). To down-regulate *GGT1* expression, RNA interference-mediated silencing was successfully applied. Subsequent screening of the generated transformants showed an efficient over 40-fold reduction in Ggt1 activity in these supernatant fractions (Fig. 4B). One of the *GGT1*-overexpressing strains (OE) and three of the *GGT1* RNAi-silenced mutants (#1.29, #1.49, and #2.8) were chosen and their ability to reduce ferric iron in cultures was then assayed. Comparing to control, cultures of the Ggt1-overproducing strain possessed nearly three-fold higher GGT activity, whereas supernatants from the selected RNAi mutants #1.29, #1.49, and #2.8 had only 6.3, 6.1, 3.6 % of GGT activity in the corresponding control, respectively (Fig. 5A). Subsequent chromatographic analyses of supernatant proteins obtained from those mutants' cultures demonstrated changes in intensities of the Ggt1-corresponding peaks, which correlated with the observed levels of the enzymatic activity (data not shown). GSH-dependent iron reductase activity was also assessed in these strains. In general, the altered patterns in *GGT1* expression/activity corresponded to almost the same changes in GSH-FeR activity (Fig. 5B). RNAi-mediated downregulation of Ggt1 activity resulted in a decreased GSH-dependent extracellular iron reduction, which in the three selected RNAi transformants amounted to only 14.6, 15.0, and 3.0 % of the activity observed in wild type. Upregulation of Ggt1 activity had the opposite effect and yielded about a 3.6-fold increase in GSH-FeR activity in culture supernatants. These results establish a link between Ggt1 and extracellular ferric iron reduction by *H. capsulatum*.

Insights into a mechanism of Ggt1-assisted extracellular iron reduction in H. capsulatum

To confirm that Ggt1 activity was responsible for these findings, a set of classical GGT inhibitors, such as serine/borate complex (SBC), 6-diazo-5-oxo-L-norleucine (DON), and acivicin, was tested (Table 3). In addition, we also examined effects of non-reducible iron analogues, such aluminum and gallium, which are recognized as potent GSH-FeR inhibitors, on both glutamyltransferase and ferric reductase activities. Prior to each enzymatic reaction, the enzyme preparation was pretreated with individual inhibitors (used at 0.1 mM concentration) for 15 min, after which inhibitors were removed by diafiltration and proper substrates were added.

Control reactions remained untreated. SBC, DON, and acivicin completely abolished both GpNA conversion and ferric iron reduction. Aluminum and gallium also exerted a strong inhibitory effect upon GSH-FeR activity; however no inhibitory action of these two metals was detected with reference to GGT activity. Based on these observations, we concluded that extracellular ferric iron reduction in *H. capsulatum* is a two-step process with an initial step catalyzed by Ggt1 and followed by the ferric iron reduction one.

As the secreted ferric reductase of *H. capsulatum* exerts its activity only when GSH is present, we hypothesized that the Ggt1-catalyzed process of extracellular iron reduction somehow involves utilization of GSH. In fact, GSH as a tripeptide consisting of γ-glutamyl, cysteinyl and glycinyl residues is an excellent physiological substrate, which can be efficiently metabolized by eukaryotic GGT-type enzymes (Penninckx and Jaspers, 1985; Mehdi *et al.*, 2001; Csala *et al.*, 2003). To verify this assumption, we examined the composition of products generated from GSH during the course of the *H. capsulatum* Ggt1-catalyzed reaction using chromatographic and spectrometric approaches. Mass spectrometry analysis revealed a significant decrease in GSH content accompanied by an additional molecular peak corresponding to the molecular mass of cysteinylglycine (data not shown). Interestingly, a molecular peak representing a glutamylglycylglycine tripeptide could be scarcely observed in transpeptidation-type reaction mixtures amended with glycylglycine. A lack of abundant amounts of glutamylglycylglycine does not mean this tripeptide was not generated in the reaction course, but rather indicates its relatively tentative nature in the presence of Ggt1 and

also results from a low efficiency of transpeptidation. With all probability, this short tripeptide generated in small amounts underwent a subsequent GGT-catalyzed conversion into glycylglycine and simultaneous glutamyl residue transfer onto a water molecule. In fact, two distinct molecular peaks corresponding to these two chemicals could be seen on mass spectrometry chromatograms (data not shown). This finding is in good agreement with our above-described observations confirming that the *H. capsulatum* Ggt1 preferentially catalyzes hydrolysis-type reactions. Overall, GSH could be converted into cysteinylglycine in the presence of *H. capsulatum* Ggt1.

GSH is an important and abundant antioxidant, which can reduce ferric iron. The reduction process involves a highly reactive thiol group of cysteine. On the other hand, cysteinylglycine, the product of Ggt1-catalyzed GSH conversion, also possesses this thiol group and should possess similar reductive properties. To verify this hypothesis, the ability of both substances to reduce iron was determined. GSH and its GSH-derived dipeptide were used at concentrations up to 10 mM. As shown in Fig. 6A, cysteinylglycine at as low a concentration as 0.5 - 1 mM (which was normally utilized throughout the entire study) generated measurable amounts of ferrous iron, whereas only slight iron reducing activity was observed with 1 mM GSH. In fact, the ability of 1 mM cysteinylglycine to reduce iron was over 117-fold higher when compared to the activity of 1 mM GSH (Fig. 6B). The differences in iron reduction activity between GSH and cysteinylglycine could be due to distinct three-dimensional structures of both compounds, which directly determine variable access to the thiol groups in those chemicals. In GSH, the thiol group is located in the middle of the molecule and is surrounded by two amino acid residues. This situation is different in cysteinylglycine, where the thiol group of cysteine is surrounded by only one glycine residue and, thereby, remains more sterically available to potential oxidized substrates.

To test whether the thiol group within the cysteinyl residue is involved in iron reduction, we examined various derivatives of GSH with different modifications of either thiol or other functional chemical groups in their structures (Fig. 6B). All the chemicals were tested at 1 mM concentration. Iron reduction activity could be easily detected when compounds bearing free SH, such as GSH or its ethyl ester (GSHEt), were studied. On the other hand, no ferrous iron was generated when oxidized derivatives of GSH, such as oxidized glutathione (GSSG) or *S*-methylglutathione (GSMe), were tested. These results indicated the thiol group was indispensable for iron reduction to occur. Interestingly, iron reduction activity of the cysteinylglycine dipeptide was inhibited in the presence of trivalent aluminum and gallium ions (Table 3). This inhibitory action could be overcome by raising ferric iron concentration (Liesener *et al*., 2004), which indicated a competitive nature of these two metal inhibitors. In fact, iron and its non-reducible trivalent analogues are able to form relatively stable complexes with thiol-containing amino acid and short oligopeptides (Farkas and Sovago, 2002).

Kinetics of the Ggt1-assisted extracellular iron reduction in H. capsulatum

To evaluate the efficacy of Ggt1-assisted iron reduction as a function of pH and to determine the efficiency of Ggt1-catalyzed decomposition of GSH (which is equivalent to release ratios of cysteinylglycine from GSH), we applied the following approach. Firstly, we measured the total iron reduction capability of this reaction system (with both Ggt1 and GSH added). Then, we determined the extent of iron reduction by cysteinylglycine alone. Both determinations were carried out in a broad pH range from 5.5 to 8.5, which enabled detailed calculations of kinetic parameters of the Ggt1-catalyzed reaction of GSH hydrolysis. Total iron reduction activity was almost constant in the range of pH values examined and a diminutive, but statistically insignificant trend toward decreasing this activity at higher pH could be observed (Fig. 7). The maximal iron reduction of 1.09 ± 0.05 μmol of Fe^{2+} min^{-1} (mg Ggt1)$^{-1}$ was determined in our test at pH 5.5, whereas the lowest amounts of reduced ferrous iron (0.84 ±

0.06 μmol of Fe^{2+} min^{-1} (mg Ggt1)$^{-1}$) were measured at pH 8.5. This even level of iron reduction activity at different pHs resulted from differences in activities of both Ggt1 and cysteinylglycine. The latter was mostly active in acidic environments (2.85 ± 0.08 μmol of Fe^{2+} min^{-1} (mmol CysGly)$^{-1}$ at pH 5.5) and considerably less efficient as an iron-reducing factor under neutral and alkaline conditions (0.96 ± 0.08 μmol of Fe^{2+} min^{-1} (mmol CysGly)$^{-1}$). The opposite situation was observed with reference to the Ggt1 activity characteristics computed with GpNA (as reported in Fig. 3). The same Ggt1 activity pattern could be observed in the case of GSH hydrolysis. This reaction was optimal at pH above 7.5 and released up to 0.88 ± 0.03 mmol of cysteinylglycine min^{-1} (mg Ggt1)$^{-1}$ (which is equivalent to decomposition of the same amount of GSH). Based on these findings, we concluded that the reaction catalyzed by cysteinylglycine was rate limiting at higher pH and was compensated by an increase in Ggt1 activity, and *vice versa* at lower pHs. Overall, the data indicated that the efficiency of extracellular iron reduction in *H. capsulatum* resulted from a combination of both reactions complementing one another in this process.

Ggt1 and H. capsulatum in vitro growth and virulence

To determine whether Ggt1 contributes to the *H. capsulatum* virulence, we firstly assayed the panel of created *GGT1*-mutant strains for growth at 37°C in HMM, a rich defined medium. Equal numbers of yeast cells taken from late-log-phase cultures (as determined for wild type) were grown for 4 days and culture turbidity was monitored in 12 h intervals. Alterations in *H. capsulatum* Ggt1 activity caused substantial defects in *in vitro* growth of both *GGT1* overexpressing and RNAi silenced mutants (Fig. 8A). Although all cultures achieved the same final turbidity, log-phase growth rates of the *GGT1* overexpressing strain were reduced approximately by 22-25 % relative to the wild-type control, whereas the RNAi mutants showed about 34-37 % reduction in log-phase growth. Because these *H. capsulatum* strains grew *in vitro* at different rates, we utilized growth phase-normalized yeast cultures in infection assays. We determined relative virulence by infecting murine macrophage-like RAW 264.7 cells with the *H. capsulatum* strains and subsequently measuring host cell death. Alterations in Ggt1 activity correlated with *H. capsulatum* virulence in this infection model. Compared to uninfected macrophage controls, both wild type and empty vector control strains caused substantial damage to macrophage monolayers (shown as WT in Fig. 8B). Relative to these WT controls, the *GGT1* overexpressing mutant appeared more virulent despite its reduced growth rate alone in HMM, whereas RNAi downregulation of *GGT1* yielded significant deficits in virulence (Fig. 8B). Similar results were obtained in five independent experiments.

Discussion

In this study, the *H. capsulatum*-secreted Ggt1 enzyme was purified to homogeneity and its enzymatic properties including iron reduction activity were examined. In the course of the purification procedure, no other fraction was found to exhibit iron reduction activity in all purification steps. Importantly, the presence of this activity was always co-detected with glutamyltransferase activity. On SDS-PAGE gels, the purified *H. capsulatum* GGT1 appeared as two glycosylated peptide subunits, which is a well-recognized feature of all known GGTs, also those isolated from fungi (Penninckx and Jaspers, 1985). Previously published studies have demonstrated mammalian and bacterial GGTs to be synthesized as a pro-GGT and subsequently processed into a large and a small subunit (Boanca *et al.*, 2006; 2007). This event occurs only after early cleavage of the pre-pro-GGT, which results in removal of the signal peptide and initiates further maturation autoprocessing (Boanca *et al.*, 2006; 2007). Large and small protein subunits then fold properly to form a mature enzyme (Suzuki and Kumagai, 2002; Okada *et al.*, 2006). The presence of both large and small subunits in *H. capsulatum* Ggt1 may indicate the enzyme undergoes propeptide autoprocessing similar to those observed in mammals, bacteria and in fungi (Suzuki and Kumagai, 2002; Okada *et al.*, 2006; Boanca *et*

al., 2006; Boanca *et al.*, 2007). As the secreted Ggt1 of *H. capsulatum* appeared as a large ~320-kDa enzymatic complex, we concluded that its quaternary structure may consist of four heterodimeric polypeptide subunits, but more detailed biochemical studies are required to verify this assumption. It is very likely that proper protein subunit folding within this enzymatic complex is required to retain its activity (Zarnowski and Woods, 2005).

H. capsulatum Ggt1 exhibits comparable hydrolysis rates of the artificial substrate GpNA with the rates observed with GGTs isolated from other organisms (Schomburg *et al.*, 2004). Interestingly, Ggt1 of *H. capsulatum* mostly carries out the hydrolytic activity, whereas its transpeptidase activity was definitely less efficient. Such a specific enzymatic profile was observed also in bacterial GGT-type enzymes and is distinct from mammalian GGTs, which have a clear preference for transpeptidation (Boanca *et al.*, 2006). On the other hand, the extracellular localization of *H. capsulatum* Ggt1 distinguishes this fungal protein from the majority of other known microbial GGT enzymes, which have been mainly detected in the periplasmic space (Suzuki *et al.*, 1986) or within biological membranes (Mineyama *et al.*, 1995). Since the presence of GGT activity has been occasionally reported in cell cultures (Tomita *et al.*, 1988; Minami *et al.*, 2003), this peculiarity is considered distinctive, albeit not unique.

Although the importance of GGT in mammalian organisms has been well recognized (Orlowski and Meister, 1970; Tate and Meister, 1981; Emdin *et al.*, 2003), there are only several reports potential physiological functions of these enzymes in microbial species. GGT has been implicated in gut colonization by *H. pylori* and in the progression of diseases resulting from infection by these bacteria (Chevalier *et al.*, 1999; McGovern *et al.*, 2001). The enzyme has also been implicated in induction of apoptosis processes in *H. pylori*-infected gastric epithelial cells (Shibayama *et al.*, 2003). In general, GGT has been recognized as an important enzyme responsible for intracellular GSH turnover that contributes to nitrogen and sulfur metabolic pathways (Elskens *et al.*, 1991; Springael and Penninckx, 2003). Indeed, Suzuki *et al.* (1993) and then Shibayama *et al.* (2007) showed that utilization of either exogenous γ-glutamyl peptides by *E. coli* or glutamine and glutathione by *H. pylori* was dependent upon GGT activity. In our study, the purified *H. capsulatum* Ggt1 shared some enzymatic properties with other known GGTs, but also was different from any of the enzymes that have been reported to possess iron reductase activities. Genetic manipulations of the *GGT1* expression leading to either upregulation or downregulation of the corresponding glutamyltransferase activity concurrently resulted in a significant increase or in a significant decrease in iron reducing activity in *H. capsulatum* cultures, indicating that Ggt1 functions as a leading factor in extracellular iron reduction in this pathogenic fungus. The ferric reduction activity could also be abolished in the presence of classical GGT inhibitors, such as SBC, DON, or acivicin, which provide a link between these two activities. Additional tests involving aluminum and gallium ions demonstrated iron reduction to be a complex two-step process. To the best of our knowledge, the iron reduction-associated function of *H. capsulatum* Ggt1 is a newly identified physiological role for GGT-type proteins. As it has been reported that GSH-dependent iron reduction activity is common to all *H. capsulatum* var. *capsulatum* and *H. capsulatum* var. *duboisii* strains and also to three other species of dimorphic zoopathogenic fungi, including *Blastomyces dermatitidis*, *Paracoccidioides brasiliensis*, and *Sporothrix schenckii* (Zarnowski and Woods, 2005), our results would suggest that all these species utilize secreted GGT enzymes to generate reduced iron.

The efficiency of Ggt1-catalyzed iron reduction in *H. capsulatum* was assessed under acidic and neutral environments, because the fungus faces these pH conditions in the course of infection in a unique phagosomal or phagolysosomal compartment within pulmonary macrophages (Newman *et al.*, 2006). In our previous paper we have shown that the enzymatic ferric iron reduction activity in *H. capsulatum* G217B cultures was similar over a broad pH

range (Zarnowski and Woods, 2005). In this study, we examined the process of Ggt1-assisted ferric iron reduction in the presence of GSH, which provided the results consistent with our previous observations. Based on our findings as well as relevant information from other published studies we propose a model of extracellular iron reduction in *H. capsulatum*, which is depicted in Fig. 9. This model includes two essential reactions. The first step is strictly enzymatical and requires the presence of both GSH and Ggt1. GSH is the major thiol found in animal cells at millimolar levels and is one of the most abundant glutamyl peptides existing in nature, which is a potential source of nitrogen and sulfur (Meister and Anderson, 1983; Wu *et al.*, 2004). This ubiquitous substance is also present in macrophages at concentration ranging up to 10 mM (Rosenblat and Aviram, 1998), which potentially makes GSH available to *H. capsulatum* during infection. In fact, lung tissues are the richest in GSH in the human body, where this thiol is present at levels about 100 times higher than those observed in plasma (Rahman and MacNee, 1999). In the first step, secreted Ggt1 initiates the enzymatic breakdown of extracellular GSH by cleavage of the γ-glutamyl bond and releasing cysteinylglycine. In the second step, the thiol group of the released cysteinylglycine dipeptide interacts with ferric ions and this interaction results in generation of ferrous iron. Both reactions contribute to the efficiency of iron reduction and each step may become rate limiting under certain circumstances; however, the resultant total iron reduction activity of this system is generally constant in a broad pH range. This phenomenon results from a deft combination of kinetic parameters of both reactions involved in this process. Cysteinylglycine is mostly active at lower pH, whereas its low activity at neutral and slightly alkaline conditions is compensated by higher Ggt1 activity rates and is accompanied by more intensive release of this dipeptide from GSH. Conversely, Ggt1 is less active at lower pH, and thereby generates less molecules of cysteinylglycine, which in turn are more active in acidic environments and balance the iron reduction yield. This finding indicates that the process of iron reduction may occur under *H. capsulatum* infection-related conditions in the host macrophages. Our recent studies showing a definite preference of *H. capsulatum* yeast cells to acquire iron in its reduced more soluble ferrous form also support this statement (Zarnowski *et al.*, 2008a).

Alterations in *H. capsulatum* Ggt1 activity caused substantial defects in *in vitro* growth rates of both *GGT1* overexpressing and RNAi silenced mutant strains in the defined rich medium HMM. Our attempt to complement the observed *in vitro* growth defect by providing extra amounts of ferrous or ferric or transferrin-bound iron failed to restore growth rates of the mutants (data not shown). Our findings suggest that the observed *in vitro* growth differences are due to a *GGT1* over- or underexpression effect unrelated to iron, which is not surprising given the potential roles of the enzyme in redox reactions as well as nitrogen and sulfur metabolism. This idea is supported by the relatively high K_m values reported in this study. If the K_m for the Ggt1-catalysed decomposition of GSH were low, this enzymatic process would be too intense and would result not only in decreased GSH amounts, but would also lead to proportionate accumulation of CysGly followed by excessive iron reduction in the *Histoplasma*-infected macrophages. Thus, the redox balance within this unique microenvironment would be impaired. In fact, it is likely that this phenomenon occurs in the *GGT1* overexpressing mutant, thereby underlying the observed growth defect in this strain.

Previous studies by Chevalier *et al.* (1999) and then McGovern *et al.* (2001) have demonstrated GGT as one of a number of virulence factors produced by *H. pylori*. As *H. capsulatum* is an intracellular pathogen, we determined contribution of Ggt1 to virulence using the murine macrophage-like RAW 264.7 cell line as an infection model. Our experiments to overexpress or underexpress *GGT1* provided evidence linking Ggt1 activity levels to *H. capsulatum* virulence. The *GGT1* overexpressing strain killed more macrophages *in vitro* than wild type or empty vector control strains, whereas this macrophage killing capability was significantly reduced in the *GGT1* RNAi mutants. We have not been able to design a way to measure the efficiency of Ggt1-assisted iron reduction under *in vivo* conditions. However, there is evidence

that this process does occur during macrophage infection. We could detect GGT activity in cultures of macrophages infected with live *H. capsulatum*, but not uninfected macrophage cultures or cultures inoculated with heat-killed fungal cells (data not shown). The kinetic properties of this enzymatic activity were the same as determined for *H. capsulatum* Ggt1 (data not shown), which is consistent with production of this enzyme by the pathogenic fungus in infected RAW 264.7 macrophages. We did not detect evidence for mammalian GGT activity, although it may have been present below our detection limit. Moreover, macrophages contain up to 10 mM GSH (Wu *et al.*, 2004). It is also well known that there is glutathione efflux from nearly all mammalian cells, including phagocytizing macrophages (Rouzer *et al.*, 1982b). Indeed, macrophages secrete large amounts of GSH and arachidonic acid metabolites when challenged with inflammatory stimuli (Rouzer *et al.*, 1982a). The concentration of intra- and extracellular GSH pools in *H. capsulatum*-infected macrophages has not been reported, but is likely that GSH remains available to the fungus during infection at concentrations high enough to maintain the maximal activity of the Ggt1 enzymatic complex. Finally, the recent report of *H. capsulatum* secretory vesicles (Albuquerque, et al., 2008) provides a potential mechanism for extracellular transport and delivery of concentrated enzymes, which in the case of Ggt1 would foster the generation of CysGly and consequent reduction of iron.

In conclusion, we have described here a novel enzymatic iron reduction tactic exploited by *H. capsulatum* and identified Ggt1 as a key enzyme in this process. Our findings provide an exceptional insight into *H. capsulatum* iron acquisition strategies, and reveal a unique aspect of GGT function in this and other dimorphic mycopathogens of humans.

Experimental procedures

Fungal strains and growth conditions

The G217B strain (ATCC 26032) of *H. capsulatum* var. *capsulatum* Darling was used in this study. Unless specified, the fungus was maintained in a rich defined *Histoplasma*-macrophage medium broth (HMM) (Worsham and Goldman, 1988). All cells were grown in a 5 % CO_2-95 % air atmosphere. For growth curve analysis, yeast cells were taken from late-log-phase cultures and resuspended at a concentration of 3×10^5 cells/ml in 20 ml of HMM (A_{600} of 1 corresponds to 2.24×10^8 CFU/ml) (data not shown). Culture turbidity was monitored with a Klett-Summerson photoelectric colorimeter (Manostat Corporation, New York, NY).

Purification of GSH-FeR

1.5 l batch fungal cultures were grown in 2.5 l Erlenmeyer flasks in *Histoplasma capsulatum* Minimal Medium (HcMM) broth for 5 days (Zarnowski *et al.*, 2008b). The supernatant (total of 18 l) was filter-sterilized and concentrated down to about 100 ml using a Vivaflow 200 unit (Sartorius AG, Goettingen, Germany) equipped with a hydrosart 30-kDa cut-off membrane. A final concentration of high-molecular-mass fractions to about 20 ml was achieved using Vivaspin 20 units equipped with polyethersulfone 5-kDa nominal molecular mass cut-off limit membranes (Sartorius). All chromatographic separation steps were performed at room temperature on the high-performance liquid chromatography ÄKTA-Purifier 10 system (Amersham Biosciences AB, Uppsala, Sweden). All buffers used were filtered through 0.2 μm nylon membrane filters (Nalgene, Rochester, NY). Protein amounts were assessed using the BCA Protein Assay Kit (Pierce Biotechnology, Rockford, IL), with bovine serum albumin as a standard. The sample was chromatographically desalted on a HiPrep™26/10 Desalting column (Amersham) and then separated on an anion exchanger HiPrep™ 16/10 DEAE FF column (Amersham) equilibrated with 20 mM Tris/HCl (pH 8.0). Elution was carried out in a 20 mM Tris/HCl (pH 8.0)/1.0 M NaCl buffer system and proteins were eluted at a flow rate of 1 ml min^{-1} in a linear gradient of salt from 0 to 30 % in 25 column volumes. GSH-FeR positive fractions were pooled together, concentrated and applied to gel filtration on a HighPrep 16/60

Sephacryl™ S-300 HR column (Amersham) equilibrated with PBS. Proteins were eluted at a flow rate of 0.5 ml min^{-1} and 1 ml fractions were collected. Fractions containing GSH-FeR activity were concentrated and desalted on the HiPrep™26/10 Desalting column, and subsequently separated in anion exchange chromatography on a MonoQ™ 5/50 GL column (Amersham) equilibrated with 20 mM bis-Tris/HCl (pH 6.5). Proteins were eluted at a flow rate of 1 ml min^{-1} in the same buffer containing 0.5 M NaCl in an extended linear gradient from 0 to 45 % in 90 column volumes. GSH-FeR-positive fractions were collected, concentrated and separated in gel filtration chromatography on two Superdex™ 200 10/300 GL columns (Amersham) set in a row. The columns were preequilibrated with PBS and proteins were eluted in 2.2 column volumes of this buffer at a flow rate of 0.5 ml min^{-1}. Fractions containing the purified protein were filter-concentrated and resuspended in a small volume of Protein Stabilizing Cocktail (Pierce). The enzyme was stable for at least 6 months when stored at 4°C.

In addition, a pool of purified GSH-FeR was subjected to chromatofocusing on a MonoP™ 5/200 GL column (Amersham). Proteins were separated in a linear pH gradient in a range of 7-4 in two buffer systems: 25 mM bis-Tris, pH 7.1 was utilized as a starting buffer, and 10 % (v/v) Polybuffer 74, pH 4.0 was applied in a protein elution step. Both buffers were adjusted to desired pH values with a saturated solution of iminodiacetic acid.

Internal amino acid sequencing

The trypsin digestion procedure used is a modified version of the protocol published elsewhere (Shevchenko *et al.*, 1996). GSH-FeR-positive fractions transferred into a 1.5-ml Eppendorf tube were reduced with 150 μl of 100 mM NH_4CO_3 and 10 μl of 45 mM DTT for 30 min at 60°C, and subsequently alkylated with 10 μl of 100 mM iodoacetic acid for 20 min. The solvent was removed in a rotary evaporator and the dried samples were rehydrated with a digestion solution consisting of 30 μl of 100 mM NH_4HCO_3 containing 0.3 μg sequencing grade modified trypsin (Promega, Madison, WI). The reaction was carried out at room temperature overnight and subsequently subjected to nanospray LC-tandem MS analysis. Samples were loaded onto a monolithic in-house fabricated capillary column (Polymicro Technologies, Phoenix, AZ) packed with Aquapore C_{18} media (Applied Biosystems, Inc., Foster City, CA). All mass spectra were obtained on a Finnigan LCQ Deca XP Ion Trap mass spectrometer (ThermoFinnigan, San Jose, CA). Data were acquired in a data-dependent manner (dynamic exclusion repeat count of 2 and repeat duration of 1 min) using a triple play method, in which a full scan was followed by a zoom scan and tandem MS of the most abundant ion in that scan. In the absence of a completed database for *H. capsulatum*, all tandem MS spectra were manually examined and interpreted for sequence information. In some cases, derived sequences were searched for similarity profiles with related fungal genomes using BLAST (Basic Local Alignment Search Tool).

Enzymatic assays

GGT activity of the purified enzyme was determined in a microtitre plate-based assay using a synthetic substrate GpNA as the donor of the γ-glutamyl residue. In the transpeptidation-type reaction, 20 mM glycylglycine was used as an acceptor substrate. The total reaction volume was 150 μl. The reaction was carried out in PBS (except where noted) at 37°C and then amounts of released *p*-nitroanilide were determined spectrophotometrically at 412 nm. To determine kinetics parameters of Ggt1-catalyzed GpNA decomposition, the substrate was used at concentrations up to 2.67 mM. The K_m and V_{max} values with their standard deviations were calculated for all the enzyme assays by a non-linear least squares regression fit of the measured (v, [S]) values to a hyperbola using the PRISM software (GraphPad Software, San Diego, CA). Standard deviations calculated were in general less than 8 % of derived parameter values, indicating a good fit of the data to the Michaelis–Menten relationship. To determine the effect

of pH upon Ggt1 activity, 150 mM MES (pH 5.5-6.5) and 150 mM HEPES (pH 7.0-8.5) were used.

Iron reduction activity was determined with GSH or cysteinylglycine in a microtitre plate-based assay as described elsewhere (Zarnowski and Woods, 2005). Total iron reduction activity of the studied system was determined with Ggt1 and GSH added, and ferric nitrate chelated with an equal molar ratio of nitrilotriacetic acid was used as a substrate. The formation of ferrous ions was quantified with the chromogenic chelator ferrozine (Sigma). The total reaction volume was 120 μl. The reaction was carried out in PBS (except where noted) at 37°C and then the absorbance was measured at 562 nm. The negative control contained all appropriate compounds and no non-enzymatic iron reduction was observed under the conditions described above. To determine the effect of pH upon iron reduction activity, 150 mM MES (pH 5.5-6.5) and 150 mM HEPES (pH 7.0-8.5) were used. To establish the role of thiol group in iron reduction process, GSH and its derivatives such as glutathione ethyl ester (GSHEt), oxidized glutathione (GSSG), *S*-methylglutathione (GSMe), were tested at 1 mM doses.

Ggt1-catalyzed GSH hydrolysis ratios as a function of pH were calculated as follows: Firstly, we measured the total iron reduction capability of this reaction system with both Ggt1 and GSH added as described above. Then, we determined K_m and V_{max} values with their standard deviations for cysteinylglycine-catalyzed iron reduction in different buffer systems using a PRISM-assisted non-linear regression (GraphPad Software). This step enabled us to calculate amounts of cysteinylglycine released from GSH under various pH conditions. As molar ratios of the dipeptide release and GSH decomposition are equal in this reaction, we were thereby able to determine the extent of Ggt1-catalyzed GSH hydrolysis.

0.1 mM 6-diazo-5-oxo-L-norleucine (DON), serine/borate complex (SBC), and acivicin were tested as classical GGT activity inhibitors (Tate and Meister, 1981), whereas 0.1 mM aluminum and gallium (as nitrate salts) were examined as iron reductase activity inhibitors (Zarnowski and Woods, 2005). Prior to each reaction, the reaction mix was pretreated with individual inhibitors for 15 min, after which inhibitors were removed by diafiltration and proper substrates were added.

ESI-MS analysis

Analyses of products obtained after a Ggt1-catalyzed reaction were carried out on a 3200 QTRAP tandem mass spectrometer (Applied Biosystems, Foster City, CA) equipped with a Turbo V™spray source. The sample was injected as a 10 μl aliquot at 30 μl ml^{-1} from the 4.6-mm diameter auto-syringe delivery system (Harvard Apparatus, Holliston, Massachusetts) in 50 % MeOH. The following instrumental parameters were used to generate the most optimum protonated ions [$M+H^{\oplus}$] in Positive Mode: ion spray voltage (IS), 5.5 kV; curtain gas (CUR), 20 psi; Nebulizer gas (GS1), 20 psi; turbo gas (GS2), 10psi; turbo gas temperature (TEM), 150°C; interface heater (ihe), ON; declustering potential (DP), 15 eV; entrance potential (EP), 10 eV; detector (CEM), 1,900; dwell time, 2,000 msec; pause time, 5.0 msec. Acquired data was processed using Analyst 1.4.2 software (Applied Biosystems) to deconvolute parent masses observed in the range from 100 to 1000 amu.

Genetic manipulations

Plasmids were cloned and propagated in the *Escherichia coli* strain JM109. Vectors were isolated from *E. coli* by using an alkaline lysis QIAprep8 miniprep kit procedure according to the recommendations of the kit manufacturer (QIAGEN, Valencia, CA). DNA from agarose gels was purified by using the QIAquick silica gel extraction kit (QIAGEN). DNA was isolated from *H. capsulatum* by using a MasterPure yeast DNA purification kit according to the directions of the manufacturer (Epicenter, Madison, WI). RNA was isolated from yeast cells

using a RiboPure-Yeast kit (Ambion) and Superscript III reverse transcriptase (Invitrogen) was used in the synthesis of first-strand cDNA according to the supplier's protocol. All PCR products were amplified using the high-fidelity Triplemaster polymerase (Eppendorf, Westbury, NY).

Plasmid pLBZ1 is an *H. capsulatum* expression vector derived from pWU55 (Woods *et al.*, 1998). It carries a *PaURA5* marker for selection, an inverted telomeric region for linearization and maintenance, and *Asc*I and *Sbf*I cloning sites between the *H2B* 5' and *CATB* 3' flanking sequences. Primers were designed to amplify 686 bp upstream of the *H2B* start codon, and 727 bp downstream of the *CATB* stop codon from the G217B strain of *H. capsulatum*. The two products were then mixed together and used as a template for splice by overlap extension in a PCR reaction (SOE PCR). *Asc*I and *Sbf*I sites were included on the two internal primers to create cloning sites between the *H2B* and *CATB* regulatory sequences. *Bam*HI sites were included on the two external primers, and the final SOE PCR product was cloned into the *Bam*HI site of pWU55. This plasmid was used in further genetic manipulations of *GGT1* overexpression and RNAi-mediated *GGT1* silencing.

For *GGT1* overexpression, two putative *GGT1* ORF sequences (1518-bp ORF1 and 1758-bp ORF2 shown in Fig. 1A) were amplified with two pairs of primers (*GGT1*.AscI.ORF1.F and *GGT1*.SbfI.ORF1.R for ORF1, and *GGT1*.AscI.ORF2.F and *GGT1*.SbfI.ORF1.R for ORF2, respectively) and subsequently cloned into the pLBZ1 plasmid. This step yielded two vectors, pLBZ1_OE::*GGT1*.ORF1 and pLBZ1_OE::*GGT1*.ORF2, respectively, which were subsequently electroporated into a uracil-auxotrophic *H. capsulatum* G217B*ura5-23* strain (Woods *et al.*, 1998) as described below.

For *GGT1* RNAi silencing, 1502-bp *GGT1* fragments were PCR amplified from cDNA and cloned in opposite orientations into pBluescript SK(+) (Stratagene, La Jolla, CA). The first fragment was amplified with *GGT1*.RNAi.KpnI.AscI.F1 and *GGT1*.RNAi.HindIII.R1 primers and cloned into *Kpn*I and *Hin*dIII restriction sites. The second fragment was amplified with *GGT1*.RNAi.NotI.SbfI.F2 and *GGT1*.RNAi.XbaI.R2 primers and then cloned in opposite orientation into *Not*I and *Xba*I restriction sites. *Asc*I and *Sbf*I sites were also introduced with these primers. Extra loop sequence of 151 bp amplified from the *tetR* gene on pWU55 using a pair of t-1 and t-2 primers was cloned into the *Bam*HI site for a total loop sequence of 220 bp. The entire *GGT* hairpin was excised then from the resulting plasmid pBS_*GGT1* RNAi and cloned into the *H. capsulatum* expression vector pLBZ1 yielding the pLBZ1_*GGT1* RNAi plasmid.

The G217B *ura5-23* strain was electrotransformed with both OE and RNAi-type vectors as previously described (Woods *et al.*, 1998). Briefly, cells were grown for 42 h with shaking at 37°C, washed once with 10 % mannitol, and electroporated with *Pme*I-digested, ethanol-precipitated pLBZ1_OE::*GGT1*.ORF1, pLBZ1_OE::*GGT1*.ORF2, pLBZ1_*GGT1* RNAi or pLBZ1 as an empty-vector control in a Gene Pulser electroporator (Bio-Rad, Hercules, CA). Following transformation, cells were spread onto HMM plates and grown for 2 to 3 weeks at 37°C. Following growth on plates, individual colonies were selected and grown in liquid medium. Three-day liquid cultures of 72 transformants were screened and assayed using the above-described GGT and iron reductase assays. Strains that appeared to have significantly altered Ggt1 activity levels were rescreened, and selected mutants analyzed by Southern blotting for confirmation of transformation (data not shown), and individual colonies were purified.

Virulence assay

The mammalian cell line used in this study was RAW 264.7 (ATCC TIB-71), a murine macrophage-like cell line acquired from the American Type Culture Collection. RAW 264.7

cells were grown in RPMI medium (Cellgro, Herndon, VA) supplemented with 10 % heat-inactivated fetal calf serum (Invitrogen, Carlsbad, CA). *H. capsulatum* virulence for RAW 264.7 cells was determined using a modified protocol for determination of macrophage killing as described elsewhere (Rappleye *et al.*, 2004). Briefly, monolayers of RAW 264.7 cells were plated at a density of 5×10^4 cells per well in 96-well plates and allowed to adhere overnight. Next, RAW 264.7 cells were infected with growth phase-normalized *H. capsulatum* yeast cultures at an MOI of 5:1 (yeasts : macrophages) in 96-well plates. Culture normalization was performed on the basis of the reduced *in vitro* growth rates of the *GGT1* overexpressing and RNAi strains, as determined previously. Cultures were started earlier based on the degree of growth rate reduction, adjusting to achieve the same culture turbidities and cell densities at the time of initiation of infection. The plates were placed at 37°C, and infection was allowed to progress for 4 h. After 4 h, uninternalized yeast cells were washed away with serum-free RPMI medium, and complete RPMI medium containing 10 % fetal calf serum was added to each well. The plates were then incubated for 5 days at 37°C in 5 % CO_2-95 % air. On day 5, culture medium was removed, and the remaining macrophages were lysed with a macrophage lysis solution (10 mM Tris, 1 mM EDTA, 0.05 % SDS, supplemented with Protease Inhibitor Cocktail), which liberates macrophage DNA but not yeast DNA. The remaining yeast cells were removed by centrifugation. PicoGreen double-stranded DNA quantification reagent (Molecular Probes) was used to measure the amount of released macrophage DNA in each well. Data shown were collected from five independent assays.

GGT assay of macrophage cultures

RAW 264.7 macrophages were left uninfected, inoculated with heat-killed (65°C, 10 min) *H. capsulatum* yeasts, or infected with live *H. capsulatum* yeasts by a scaled-up modification of the virulence assay described above. Briefly, 2.55×10^5 RAW 264.7 cells were seeded per cm^2 in 75 cm^2 tissue culture flasks and allowed to adhere overnight. The monolayers were then left untreated or inoculated with live or heat-killed *H. capsulatum* yeast cultures at an MOI of 5:1 (yeasts : macrophages). The flasks were placed at 37°C, and infection was allowed to progress for 4 h. After 4 h, uninternalized yeast cells were washed away with serum-free RPMI medium, and complete RPMI medium containing 10 % fetal calf serum was added to each well. The flasks were then incubated for 5 days at 37°C in 5 % CO_2-95 % air. On day 5, culture medium was removed, and the remaining macrophages were scraped off the surface, resuspended in RPMI medium and centrifuged (1200×g, 10 min). Cell pellets were lysed with the macrophage lysis solution described above and centrifuged again (1200×g, 10 min). GGT activity was determined in the resulting RAW 264.7 cell lysates according to the protocol provided above.

Statistics

For statistical analysis, Student *t*-test was used (SigmaPlot 2004 ver. 4.0, Systat Software Inc., San Jose, CA). *P* values less than 0.05 were considered significant.

Acknowledgements

We are grateful to Drs. Imre Sovago (University of Debrecen), Richard E. Cowart Jr. (University of Dubuque), Michael D. Sevilla (Oakland University) and Mr. Kurt Andersson (Amersham/GE Healthcare) for helpful discussions and comments. We thank Mr. Grzegorz Sabat for his excellent technical assistance with ESI-MS analysis. This work was supported by NIH grants NIH R01s AI52303 and HL55949 (to J. P. W.).

References

Albuquerque PC, Nakayasu ES, Rodrigues ML, Frases S, Casadevall A, Zancope-Oliveira RM, Almeida IC, Nosanchuk JD. Vesicular transport in *Histoplasma capsulatum*: an effective mechanism for trans-

cell wall transfer of proteins and lipids in ascomycetes. Cell Microbiol. 200810.1111/j.1462-5822.2008.01160.x[Epub ahead of print: April 17th, 2008]. “Postprint”

Appelberg R. Macrophage nutriprive antimicrobial mechanisms. J Leukoc Biol 2006;79:1117–1128. [PubMed: 16603587]

Boanca G, Sand A, Barycki JJ. Uncoupling the enzymatic and autoprocessing activities of *Helicobacter pylori* gamma-glutamyltranspeptidase. J Biol Chem 2006;281:19029–19037. [PubMed: 16672227]

Boanca G, Sand A, Okada T, Suzuki H, Kumagai H, Fukuyama K, Barycki JJ. Autoprocessing of *Helicobacter pylori* gamma-glutamyltranspeptidase leads to the formation of a threonine-threonine catalytic dyad. J Biol Chem 2007;282:534–541. [PubMed: 17107958]

Bohse ML, Woods JP. RNA interference-mediated silencing of the *YPS3* gene of *Histoplasma capsulatum* reveals virulence defects. Infect Immun 2007;75:2811–2817. [PubMed: 17403872]

Bullen JJ, Rogers HJ, Spalding PB, Ward CG. Natural resistance, iron and infection: a challenge for clinical medicine. J Med Microbiol 2006;55:251–258. [PubMed: 16476787]

Chevalier C, Thiberge JM, Ferrero RL, Labigne A. Essential role of *Helicobacter pylori* gamma-glutamyltranspeptidase for the colonization of the gastric mucosa of mice. Mol Microbiol 1999;31:1359–1372. [PubMed: 10200957]

Csala M, Fulceri R, Mandl J, Benedetti A, Banhegyi G. Glutathione transport in the endo/sarcoplasmic reticulum. BioFactors 2003;17:27–35. [PubMed: 12897426]

de Luca NG, Wood PM. Iron uptake by fungi: contrasted mechanisms with internal or external reduction. Adv Microb Physiol 2000;43:39–74. [PubMed: 10907554]

Elskens MT, Jaspers CJ, Penninckx MJ. Glutathione as an endogenous sulphur source in the yeast *Saccharomyces cerevisiae*. J Gen Microbiol 1991;137:637–644. [PubMed: 1674526]

Emdin M, Passiono C, Pompella A, Paolicchi A. Serum gamma-glutamyl transpeptidase: A prognostic marker in cardiovascular diseases. BioFactors 2003;17:199–205. [PubMed: 12897441]

Farkas, E.; Sovago, I. Metal complexes of amino acids and peptides. In: Barrett, GC.; Davies, JS., editors. Amino acids, Peptides and Proteins. 32. Cambridge: Royal Society of Chemistry Publishing; 2002. p. 295-364.

Foster LA. Utilization and cell-surface binding of hemin by *Histoplasma capsulatum*. Can J Microbiol 2002;48:437–442. [PubMed: 12109883]

Hiratake J. Enzyme inhibitors as chemical tools to study enzyme catalysis: rational design, synthesis, and applications. Chem Rec 2005;5:209–228. [PubMed: 16041744]

Holzberg M, Artis WM. Hydroxamate siderophore production by opportunistic and systemic fungal pathogens. Infect Immun 1983;40:1134–1139. [PubMed: 6221998]

Howard DH. Acquisition, transport, and storage of iron by pathogenic fungi. Clin Microbiol Rev 1999;12:394–404. [PubMed: 10398672]

Howard DH, Rafie R, Tiwari A, Faull KF. Hydroxamate siderophores of *Histoplasma capsulatum*. Infect Immun 2000;68:2338–2343. [PubMed: 10722639]

Hwang LH, Mayfield JA, Rine J, Sil A. *Histoplasma* requires *SID1*, a member of an iron-regulated siderophore gene cluster, for host colonization. PLoS Pathog 2008;4:e1000044. [PubMed: 18404210]

Ikeda Y, Fujii J, Anderson ME, Taniguchi N, Meister A. Involvement of Ser-451 and Ser-452 in the catalysis of human gamma-glutamyl transpeptidase. J Biol Chem 1995;270:22223–22228. [PubMed: 7673200]

Jung WH, Kronstad JW. Iron and fungal pathogenesis: a case study with *Cryptococcus neoformans*. Cell Microbiol. 2007 Nov 27; [PubMed: 18042257]Epub ahead of print

Kinlough CL, Poland PA, Bruns JB, Hughey RP. Gamma-glutamyltranspeptidase: disulfide bridges, propeptide cleavage, and activation in the endoplasmic reticulum. Methods Enzymol 2005;401:426–449. [PubMed: 16399401]

Kosman DJ. Molecular mechanisms of iron uptake in fungi. Mol Microbiol 2003;47:1185–1197. [PubMed: 12603727]

Kunkle CA, Schmitt MP. Analysis of a DtxR-regulated iron transport and siderophore biosynthesis gene cluster in *Corynebacterium diphtheriae*. J Bacteriol 2005;187:422–433. [PubMed: 15629913]

Lane TE, Wu-Hsieh BA, Howard DH. Iron limitation and the gamma interferon-mediated antihistoplasma state of murine macrophages. Infect Immun 1991;59:2274–2278. [PubMed: 1904840]

Liesener, AL.; Zarnowski, R.; Hoover, SW.; Galbraith, KM.; Jacobitz-Kizzier, JM.; Woods, JP. Ferric reduction is necessary for *Histoplasma capsulatum* utilization of iron from transferrin and in serum. Proceedings of the 104th American Society for Microbiology General Meeting; New Orleans, USA. May 23-27, 2004; 2004. Abstract F-066

McGovern KJ, Blanchard TG, Gutierrez JA, Czinn SJ, Krakowka S, Youngman P. gamma-Glutamyltransferase is a *Helicobacter pylori* virulence factor but is not essential for colonization. Infect Immun 2001;69:4168–4173. [PubMed: 11349094]

Mehdi K, Thierie J, Penninckx MJ. gamma-Glutamyl transpeptidase in the yeast *Saccharomyces cerevisiae* and its role in the vacuolar transport and metabolism of glutathione. Biochem J 2001;359:631–637. [PubMed: 11672438]

Meister A, Anderson ME. Glutathione. Annu Rev Biochem 1983;52:711–760. [PubMed: 6137189]

Mineyama R, Mikami K, Saito K. Partial purification and some properties of gamma-glutamyl peptide-hydrolysing enzyme from *Actinobacillus actinomycetemcomitans*. Microbios 1995;82:7–19. [PubMed: 7791632]

Minami H, Suzuki H, Kumagai H. Salt-tolerant gamma-glutamyltranspeptidase from *Bacillus subtilis* 168 with glutaminase activity. Enzyme Microb Technol 2003;32:431–438.

Newman SL, Gootee L, Brunner G, Deepe GS Jr. Chloroquine induces human macrophage killing of *Histoplasma capsulatum* by limiting the availability of intracellular iron and is therapeutic in a murine model of histoplasmosis. J Clin Invest 1994;93:1422–1429. [PubMed: 8163646]

Newman SL, Gootee L, Hilty J, Morris RE. Human macrophages do not require phagosome acidification to mediate fungistatic/fungicidal activity against *Histoplasma capsulatum*. J Immunol 2006;176:1806–1813. [PubMed: 16424211]

Newman SL, Gootee L, Stroobant V, van der Goot H, Boelaert JR. Inhibition of growth of *Histoplasma capsulatum* yeast cells in human macrophages by the iron chelator VUF 8514 and comparison of VUF 8514 with deferoxamine. Antimicrob Agents Chemother 1995;39:1824–1829. [PubMed: 7486926]

Okada T, Suzuki H, Wada K, Kumagai H, Fukuyama K. Crystal structures of gamma-glutamyltranspeptidase from *Escherichia coli*, a key enzyme in glutathione metabolism, and its reaction intermediate. Proc Natl Acad Sci USA 2006;103:6471–6476. [PubMed: 16618936]

Orlowski M, Meister A. The gamma-glutamyl cycle: a possible transport system for amino acids. Proc Natl Acad Sci USA 1970;67:1248–1255. [PubMed: 5274454]

Payne SM, Wyckoff EE, Murphy ER, Oglesby AG, Boulette ML, Davies NM. Iron and pathogenesis of *Shigella*: iron acquisition in the intracellular environment. Biometals 2006;19:173–180. [PubMed: 16718602]

Penninckx MJ, Jaspers CJ. Molecular and kinetic properties of purified γ-glutamyl transpeptidase from yeast *Saccharomyces cerevisiae*. Phytochemistry 1985;24:1913–1918.

Rahman I, MacNee W. Lung glutathione and oxidative stress: implications in cigarette smoke-induced airway disease. Am J Physiol 1999;277:L1067–L1088. [PubMed: 10600876]

Rappleye CA, Engle JT, Goldman WE. RNA interference in *Histoplasma capsulatum* demonstrates a role for α-(1,3)-glucan in virulence. Mol Microbiol 2004;53:153–165. [PubMed: 15225311]

Rosenblat M, Aviram M. Macrophage glutathione content and glutathione peroxidase activity are inversely related to cell-mediated oxidation of LDL: *in vitro* and *in vivo* studies. Free Radic Biol Med 1998;24:305–317. [PubMed: 9433906]

Rouzer CA, Scott WA, Griffith OW, Hamill AL, Cohn ZA. Arachidonic acid metabolism in glutathione-deficient macrophages. Proc Natl Acad Sci USA 1982a;79:1621–1625. [PubMed: 6803245]

Rouzer CA, Scott WA, Griffith OW, Hamill AL, Cohn ZA. Glutathione metabolism in resting and phagocytizing peritoneal macrophages. J Biol Chem 1982b;257:2002–2008. [PubMed: 6120172]

Runyen-Janecky LJ, Reeves SA, Gonzalez EG, Payne SM. Contribution of the *Shigella flexneri* Sit, Iuc, and Feo iron acquisition systems to iron acquisition *in vitro* and in cultured cells. Infect Immun 2003;71:1919–1928. [PubMed: 12654809]

Schomburg I, Chang A, Ebeling C, Gremse M, Heldt C, Huhn G, Schomburg D. BRENDA, the enzyme database: updates and major new developments. Nucleic Acids Res 2004;32:D431–433. [PubMed: 14681450]

Shevchenko A, Wilm M, Vorm O, Mann M. Mass spectrometric sequencing of proteins silver-stained polyacrylamide gels. Anal Chem 1996;68:850–858. [PubMed: 8779443]

Shibayama K, Kamachi K, Nagata N, Yagi T, Nada T, Doi Y, Shibata N, Yokoyama K, Yamane K, Kato H, Iinuma Y, Arakawa Y. A novel apoptosis-inducing protein from *Helicobacter pylori*. Mol Microbiol 2003;47:443–451. [PubMed: 12519194]

Shibayama K, Wachino J, Arakawa Y, Saidijam M, Rutherford NG, Henderson PJ. Metabolism of glutamine and glutathione via gamma-glutamyltranspeptidase and glutamate transport in *Helicobacter pylori*: possible significance in the pathophysiology of the organism. Mol Microbiol 2007;64:396–406. [PubMed: 17381553]

Springael JY, Penninckx MJ. Nitrogen-source regulation of yeast gamma-glutamyl transpeptidase synthesis involves the regulatory network including the GATA zinc-finger factors Gln3, Nil1/Gat1 and Gzf3. Biochem J 2003;371:589–595. [PubMed: 12529169]

Suzuki H, Hashimoto W, Kumagai H. *Escherichia coli* K-12 can utilize an exogenous γ-glutamyl peptide as an amino source, for which γ-glutamyltranspeptidase is essential. J Bacteriol 1993;175:6038–6040. [PubMed: 8104180]

Suzuki H, Kumagai H, Tochikura T. gamma-Glutamyltranspeptidase from *Escherichia coli* K-12: formation and localization. J Bacteriol 1986;168:1332–1335. [PubMed: 2877975]

Suzuki H, Kumagai H. Autocatalytic processing of gamma-glutamyltranspeptidase. J Biol Chem 2002;277:43536–43543. [PubMed: 12207027]

Tate SS, Meister A. gamma-Glutamyl transpeptidase: catalytic, structural and functional aspects. Mol Cell Biochem 1981;39:357–368. [PubMed: 6118826]

Tate SS, Meister A. Serine-borate complex as a transition-state inhibitor of gamma-glutamyl transpeptidase. Proc Natl Acad Sci USA 1981;75:4806–4809. [PubMed: 33382]

Timmerman MM, Woods JP. Ferric reduction is a potential iron acquisition mechanism for *Histoplasma capsulatum*. Infect Immun 1999;67:6403–6408. [PubMed: 10569756]

Timmerman MM, Woods JP. Potential role for extracellular glutathione-dependent ferric reductase in utilization of environmental and host ferric compounds by *Histoplasma capsulatum*. Infect Immun 2001;69:7671–7678. [PubMed: 11705947]

Tomita K, Ito M, Yano T, Kumagai H, Tochikura T. gamma-Glutamyltranspeptidase activity and the properties of the extracellular glutaminase from *Aspergillus oryzae*. Agric Biol Chem 1988;52:1159–1163.

Valko M, Morris H, Cronin MT. Metals, toxicity and oxidative stress. Curr Med Chem 2005;12:1161–1208. [PubMed: 15892631]

Weinberg ED. The role of iron in protozoan and fungal infectious diseases. J Eukaryot Microbiol 1999;46:231–238. [PubMed: 10377984]

Wheat LJ. Current diagnosis of histoplasmosis. Trends Microbiol 2003;11:488–494. [PubMed: 14557032]

Woods JP, Retallack DM, Heinecke EL, Goldman WE. Rare homologous gene targeting in *Histoplasma capsulatum*: disruption of the $URA5_{Hc}$ gene by allelic replacement. J Bacteriol 1998;180:5135–5143. [PubMed: 9748447]

Worsham PL, Goldman WE. Quantitative plating of *Histoplasma capsulatum* without addition of conditioned medium or siderophores. J Med Vet Mycol 1988;26:137–143. [PubMed: 3171821]

Wu G, Fang Y-Z, Yang S, Lupton JR, Turner ND. Glutathione metabolism and its implications for health. J Nutr 2004;134:489–492. [PubMed: 14988435]

Zarnowski R, Dobrzyn A, Ntambi J, Woods JP. Ferrous, but not ferric iron maintains homeostasis in *Histoplasma capsulatum* triacylglycerides. Curr Microbiol 2008a;57:153–157. [PubMed: 18506523]

Zarnowski R, Dobrzyn A, Ntambi J, Woods JP. Neutral storage lipids of *Histoplasma capsulatum*: effect of culture age. Curr Microbiol 2008b;56:110–114. [PubMed: 17960460]

Zarnowski R, Woods JP. Glutathione-dependent extracellular ferric reductase activities in dimorphic zoopathogenic fungi. Microbiology-SGM 2005;151:2233–2240.

Abbreviations used

DON

6-diazo-5-oxo-L-norleucine

GGT
γ-glutamyltransferase

Ggt1
H. capsulatum γ-glutamyltransferase

GpNA
γ-glutamyl-*p*-nitroanilide

GSH
glutathione, γ-glutamylcysteinylglycine

GSH-FeR
glutathione-dependent ferric reductase

Hc
Histoplasma capsulatum

HcMM
Histoplasma capsulatum minimal medium

HMM
Histoplasma-macrophage medium

SBC
serine/borate complex

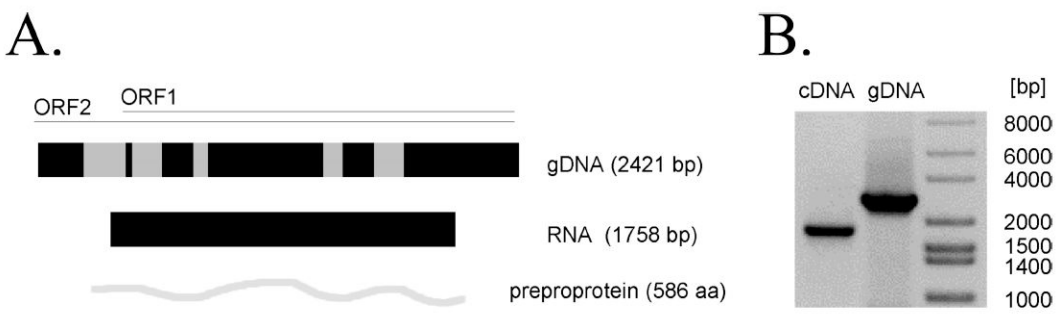

Fig. 1.

Graphical presentation of a gene encoding secreted γ-glutamyltransferase (*GGT1*) of *H. capsulatum*. (**A**) A genomic DNA sequence of *GGT1* consists of 2421 bp organized in 6 exons (in black) separated by five noncoding introns (in gray), which yield a total transcript of 1758 bp (solid black bar) and a corresponding 586-aa preproprotein (light gray bar). Solid black lines labeled as “ORF1” and “ORF2” refer to two predicted *GGT1* open reading frames. (**B**) PCR amplification of *GGT1* from genomic and cDNA templates. The gene was amplified with a pair of *GGT1*.AscI.ORF2.F and *GGT1*.SbfI.ORF1.R primers.

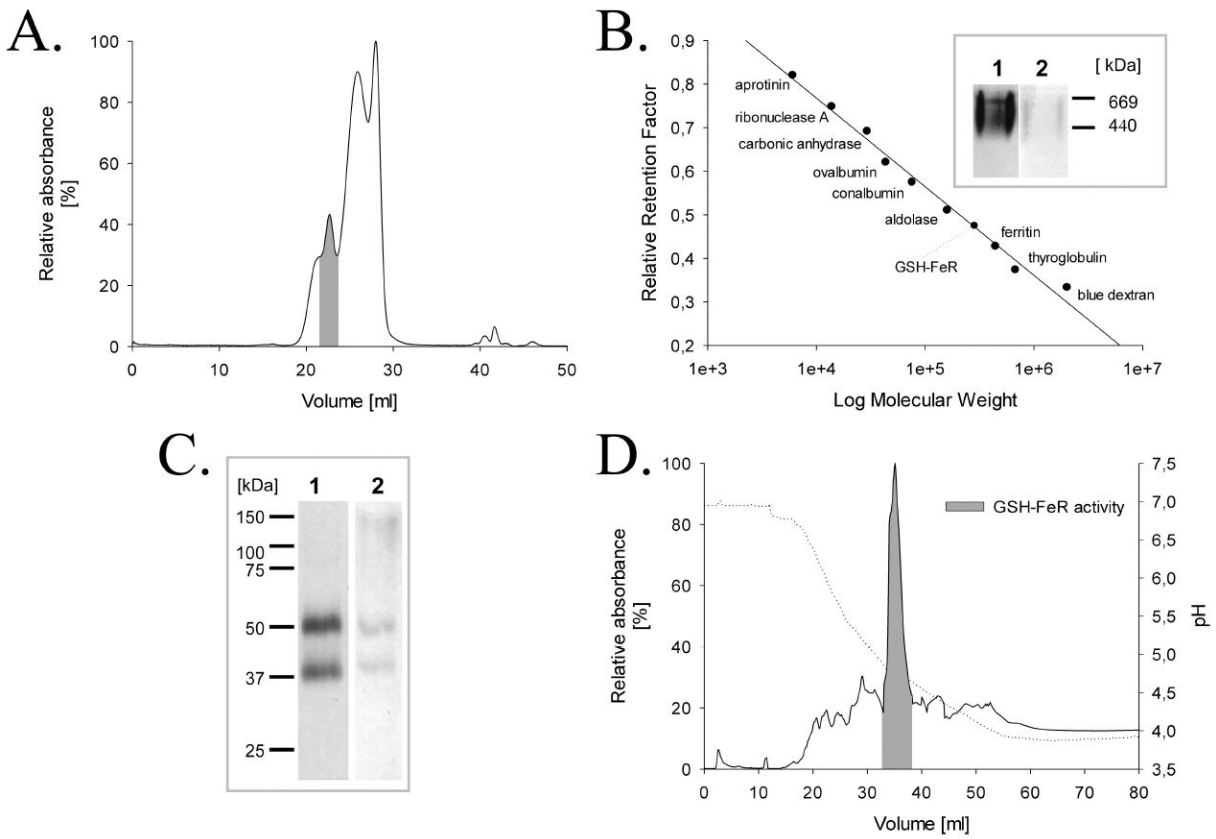

Fig. 2.

Chromatographic analysis of Ggt1 purified from *H. capsulatum* G217B culture supernatants. Proteins were detected at 280 nm. Ggt1 activity shown as a forward diagonally shaded gray area. (**A**) Purification of Ggt1 in gel filtration chromatography. Proteins were separated in PBS (pH 7.2) on two Superdex™ 200 10/300 GL columns (Amersham) set in a row. (**B**) Size exclusion column calibration with a set of protein standards: blue dextran (~2 MDa), thyroglobulin (669 kDa), ferritin (440 kDa), aldolase (158 kDa), conalbumin (75 kDa), ovalbumin (43 kDa), carbonic anhydrase (29 kDa), ribonuclease A (13.7 kDa), and aprotinin (6 kDa). Position of Ggt1 indicated by a dotted line. Inset: Electrophoretic analysis of native Ggt1 in 10 % polyacrylamide gel subsequently stained with silver (1) and for the presence of glycoproteins (2). (**C**) SDS-PAGE analysis of purified Ggt1 in 10 % denaturing discontinuous SDS-polyacrylamide gel subsequently stained with silver (1) and for the presence of glycoproteins (2). (**D**) Chromatofocusing of Ggt1 on MonoP 5/200 GL. A solid line represents an elution profile of proteins separated in a pH gradient from 7 to 4 (dotted line).

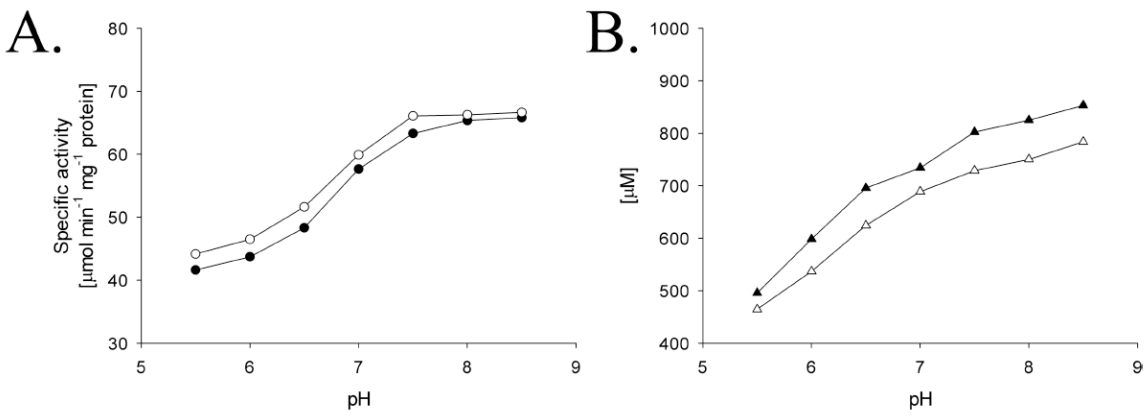

Fig. 3.

pH-dependent kinetics of the *H. capsulatum* Ggt1-catalayzed transfer and hydrolysis reactions of the artificial substrate GpNA. The maximal enzymatic activity at a saturating substrate concentration was determined in four repetitions and mean values were plotted as a function of pH. *H. capsulatum* Ggt1 was mostly active at neutral and slightly alkaline pH.(**A**) At the indicated pH values, V_{max} values for both glutamyl transfer from (●) and hydrolysis (○) of GpNA were determined. (**B**) At the indicated pH values, K_m values for both glutamyl transfer from (▲) and hydrolysis (△) of GpNA were calculated.

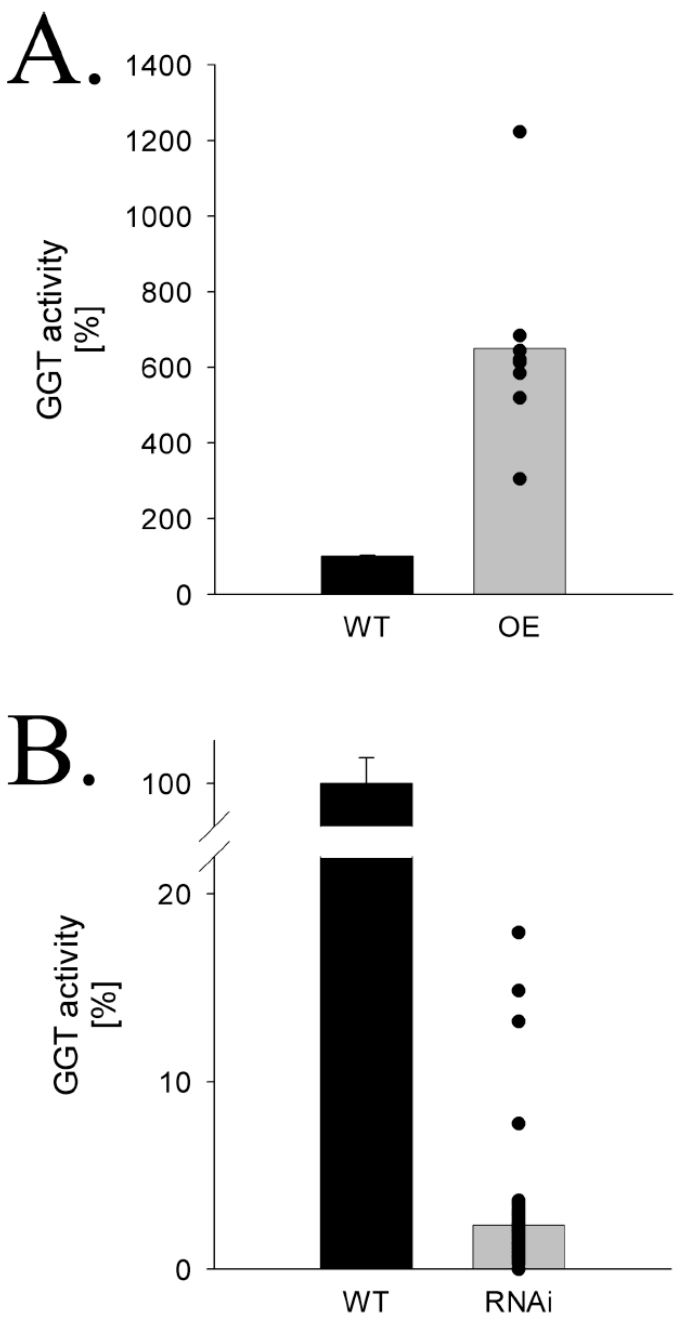

Fig. 4.

Ggt1 enzymatic activity in high-molecular weight supernatant fractions of mutants with altered *GGT1*-expression levels. Ggt1 activity levels were normalized per protein content. (**A**) Upregulation of Ggt1 activity heterologously expressed under the constitutive native *H2B* promoter. The black bar represents the level of Ggt1 activity in control, the gray bar denotes the average fold change in enzymatic activity, whereas black dots represent individual transformants. (**B**) Residual Ggt1 activity in RNAi-silenced mutants. The black bar represents the mean Ggt1 activity in control, whereas the gray bar refers to the average residual enzymatic activity in RNAi-silenced mutants, whereas each black dot represents individual transformants.

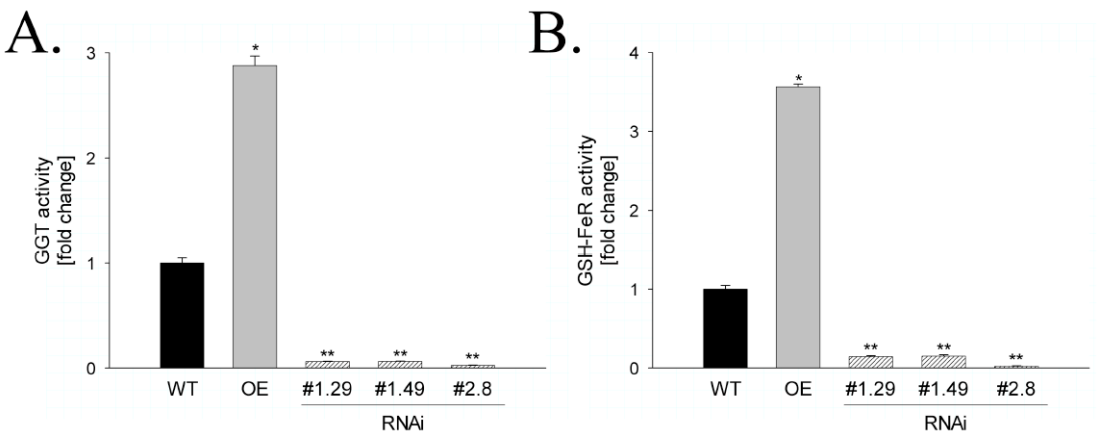

Fig. 5.

Modulation of Ggt1 activity shows concordant alterations in extracellular iron reduction in *H. capsulatum* G217B culture supernatants. Changes in Ggt1 activity (**A**) and GSH-FeR activity (**B**) were determined in culture supernatants and normalized for protein content. Data shown are from a representative of four independent experiments carried out in triplicate. * and ** indicate significant differences in enzymatic activities ($p < 0.05$) compared to WT.

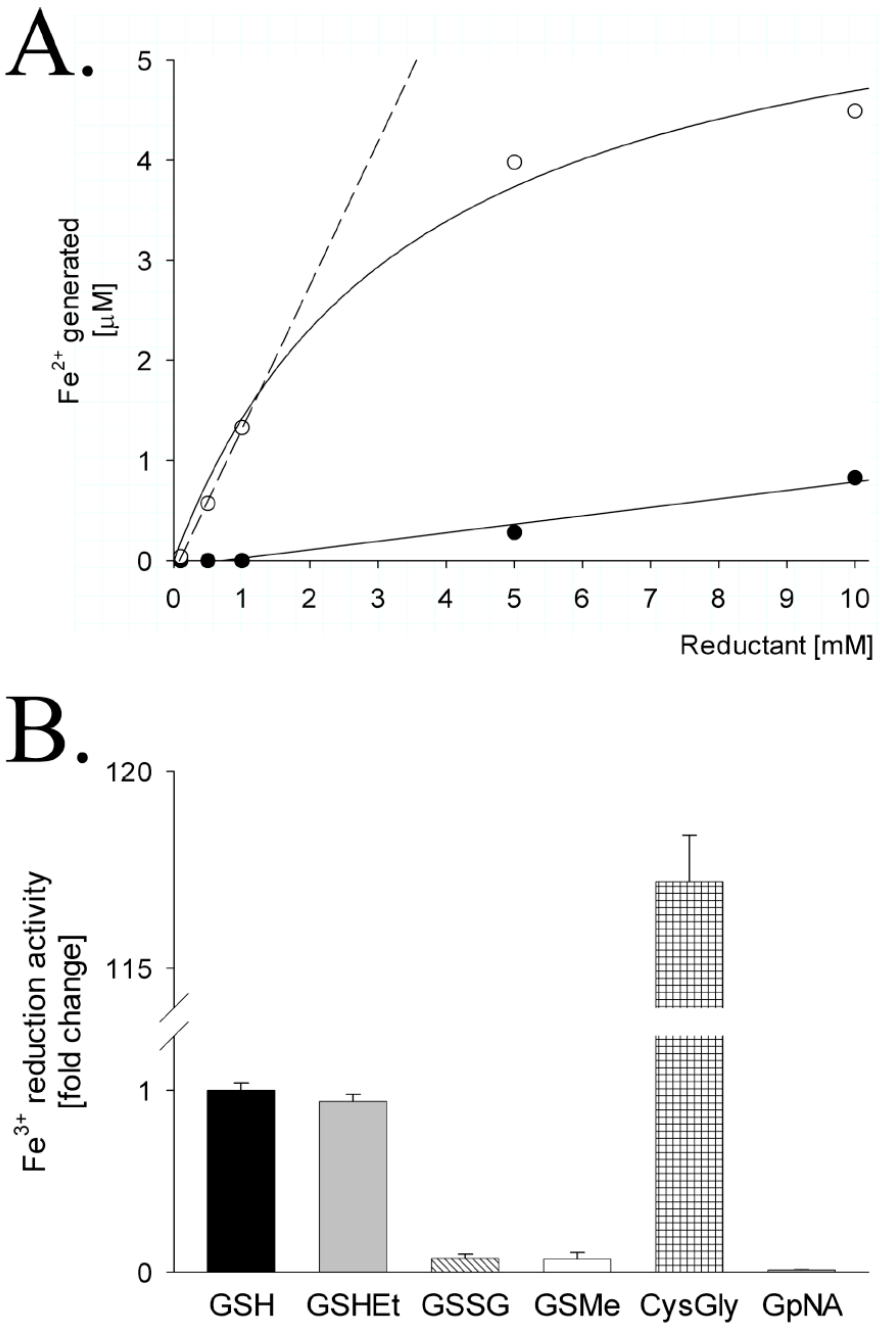

Fig. 6.

Ferric iron reducing activities of GSH (●) and CysGly (○). (**A**) Both substances were examined at concentrations up to 10 mM and amounts of generated ferrous iron were determined with ferrozine. The mean values shown are from a representative of three independent experiments carried out in triplicate. Linear regression analysis represented here demonstrated a linear correlation between iron reduction and CysGly within a concentration range of the latter up to 1.5 mM (r^2 coefficient of 0.99871). (**B**) Effects of chemical modification of GSH upon iron reduction. The substances GSH or GSH ethyl ester (GSHEt) possessed a free sulfhydryl (SH) group within a cysteine residue, whereas oxidized GSH (GSSG) and *S*-methyl-GSH (GSMe) had this group modified as a result of oxidation or alkylation, respectively. Cysteinylglycine

(CysGly), which has a free SH group, was included as an extra positive control, whereas GpNA was used as a negative one. All the tested substances were used at 1 mM concentration. The mean values shown are from a representative of three independent experiments carried out in triplicate.

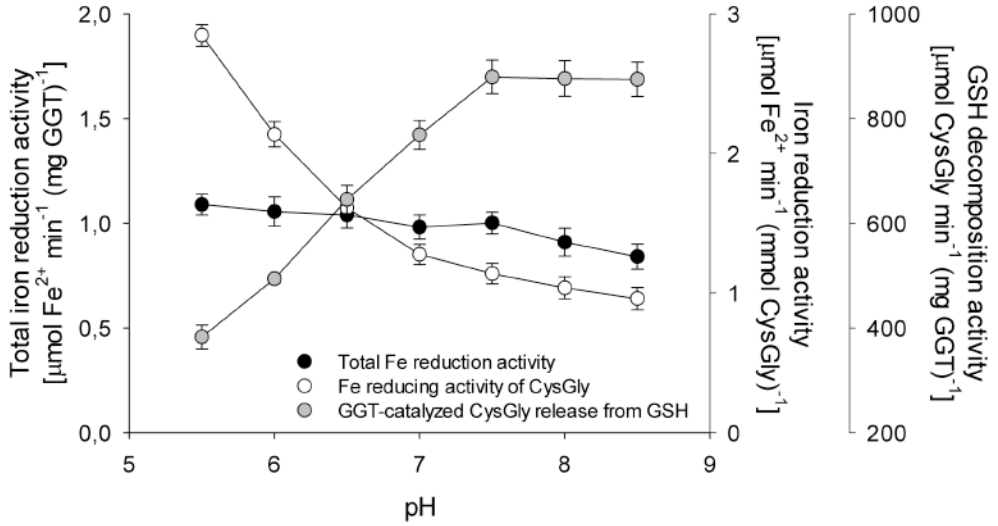

Fig. 7.

The process of Ggt1-catalyzed extracellular iron reduction is not dependent on pH due to complementary contribution of Ggt1 and cysteinylglycine activities. Total iron reduction activity is generally constant in a broad pH range and tends to decrease slightly under alkaline conditions. This phenomenon results from a deft combination of kinetics parameters of both reactions involved in this process. Cysteinylgycine is mostly active at lower pHs, whereas its low activity at neutral and slightly alkaline conditions is compensated by higher activity of Ggt1 and is accompanied by more intensive release of this dipeptide from GSH. At lower pH, Ggt1 is less active and generates less molecules of cysteinylglycine, which in turn are more active in acidic environments.

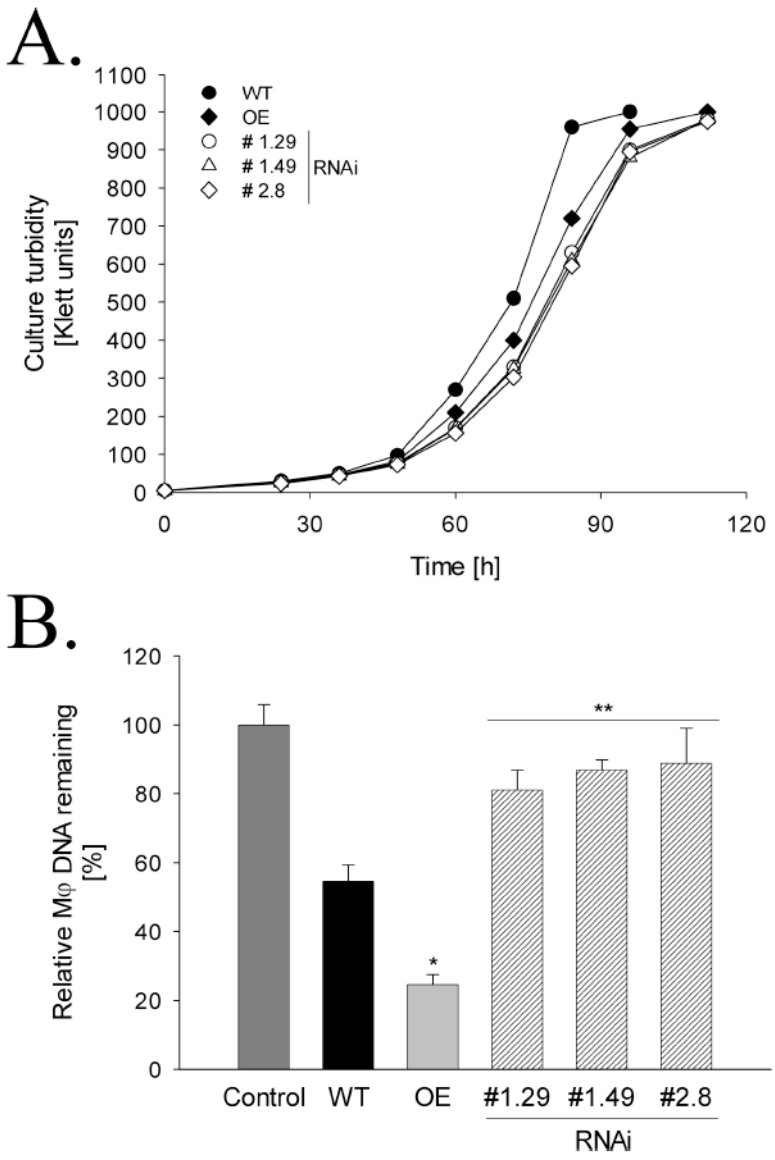

Fig. 8.

Changes in *GGT1* expression alter *H. capsulatum* growth and virulence. (**A**) *GGT1* overexpression or downregulation in RNAi mutants both impair fungal growth *in vitro* in rich defined HMM. Growth was assessed based on culture turbidity measured with a Klett-Summerson photometric colorimeter. Data are shown for a representative experiment from five independent experiments with similar results. (**B**) Variations of *GGT1* expression are correlated with the virulence of *H. capsulatum* in RAW 264.7 macrophages. Macrophage killing is determined as reductions in macrophage DNA concentration remaining after incubation of macrophages with *H. capsulatum* yeasts. Macrophage DNA remaining at 5 days after infection was compared to uninfected wells (Control). Data shown were collected from five independent assays. * and ** indicate significant differences ($p < 0.05$) compared to WT.

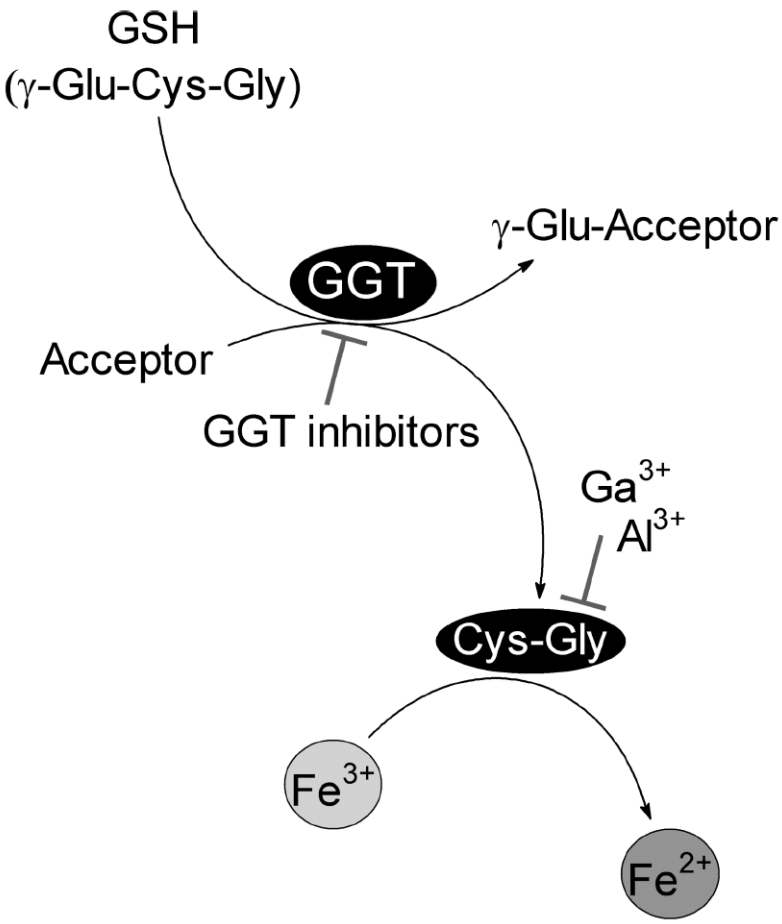

Fig. 9.

A proposed model of Ggt1-assisted extracellular iron reduction in *H. capsulatum* involves two basic reactions. The first step is strictly enzymatical and occurs in the presence of Ggt1. The enzyme converts GSH into cysteinylglycine, and classical GGT inhibitors may inhibit this step. The second reaction involves cysteinylglycine, which efficiently can reduce ferric iron. This reaction can be abolished in the presence of non-reducible trivalent aluminum and gallium ions.

Table 1

Oligonucleotides used in this study.

Oligonucleotide		Sequence[a]	Restriction site
ORF	*GGT1*.AscI.ORF1.F	NNNGGCGCGCCATGTATCATAGCGGTATCTCTGGTGG	*Asc*I
	GGT1.SbfI.ORF1.R	NNNNNNCCTGCAGGTTATTAAACAGCTCCTCCCGAATCCA	*Sbf*I
	GGT1.AscI.ORF2.F	NNNGGCGCGCCATGTTCAACCATTCCCTTGTC	*Asc*I
RNAi	*GGT1*.RNAi.KpnI.AscI.F1	NNNGGTACCGGCGCGCCACGACATTCTGGGGGAGATTG	*Kpn*I/*Asc*I
	GGT1.RNAi.HindIII.R1	NNNAAGCTTCTCTGACACATTCGGGCTAAGC	*Hin*dIII
	GGT1.RNAi.NotI.SbfI.F2	NNNNNNGCGGCCGCCCTGCAGGACGACATTCTGGGGGAGATTG	*Not*I/*Sbf*I
	GGT1.RNAi.XbaI.R2	NNNTCTAGACTCTGACACATTCGGGCTAAGC	*Xba*I
	t-1	NNNGGATCCATCGTCCATTCCGACAGCATCG	*Bam*HI
	t-2	NNNGGATCCTAGTGGCTCCAAGTAGCGAAGC	*Bam*HI

[a]Underlined sequences show the introduced restriction enzyme site in the corresponding primer.

Table 2

Summary of *H. capsulatum* Ggt1 purification.

Step[a]	Protein [mg/ml]	Total protein [mg]	GGT activity [U/ml][b]	GGT total Activity [U][b]	GGT Specific activity [U/mg][b]	Yield [%]	Fold purified
Raw supernatant	0.64	11508.18	6.1	109920	9.6	100	1
Filter-concentration	3.05	64.02	885.5	39846	622	36.3	65
DEAE	0.73	4.38	706.7	21201	4840	19.3	504
Sephacryl	0.05	2.76	378.0	20415	7397	18.6	771
MonoQ/Superdex	0.0111	0.4656	239.0	5829	12519	5.3	1304

[a] Purification from 18 l batch culture.

[b] 1 U of GGT activity generates 1 nmol pNA per min

Table 3

Effect of inhibitors on glutamyltransferase and iron reduction activities of Ggt1 and cysteinylglycine.

	Target reaction catalyzed by			
	γ-Glutamyltransferase (Ggt1)		Cysteinylglycine	
Inhibitor[a]	**Glu transfer**	**Fe^{3+} reduction**	**Glu transfer**	**Fe^{3+} reduction**
Acivicin, DON[b], SBC[b]	Inhibition	Inhibition	No effect	No effect
Aluminum, gallium	No effect	Inhibition	No effect	Inhibition

[a] Inhibitors were used at 0.1 mM concentration.

[b] DON, 6-diazo-5-oxo-L-norleucine; SBC, serine/borate complex.